Evaluation of a Praseodymium Precursor for Atomic Layer Deposition of Oxide Dielectric Films

Kaupo Kukli,*,† Mikko Ritala,† Tero Pilvi,† Timo Sajavaara,‡,¶ Markku Leskelä,† Anthony C. Jones,§ Helen C. Aspinall,§ David C. Gilmer,# and Philip J. Tobin#

University of Helsinki, Department of Chemistry, P.O. Box 55, FIN-00014 University of Helsinki, Finland, Accelerator Laboratory, P.O. Box 43, FIN-00014 University of Helsinki, Finland, Department of Chemistry, University of Liverpool, Liverpool, L69 3ZD, United Kingdom, Epichem Limited, Power Road, Bromborough, Wirral, Merseyside, CH62 3QF, United Kingdom, and Freescale Semiconductor, Inc., Advanced Products Research and Development, 3501 Ed Bluestein Blvd., Austin, Texas 78721

Received June 28, 2004. Revised Manuscript Received August 27, 2004

Amorphous PrO_x based films were grown by atomic layer deposition in the temperature range 200−400 °C from $Pr[N(SiMe_3)_2]_3$ and H_2O on *n*-Si(100) and borosilicate glass substrates. The films contained considerable amounts of residual hydrogen and residual or diffused silicon. The refractive indexes of the films varied between 1.76 and 1.87. Crystallization took place after annealing at 900−1000 °C, and X-ray diffraction data indicated that the films were $Pr_{9.33}(SiO_4)_6O_2$. The effective permittivity of 70−100 nm thick films was in the range of 14−16. Annealing at 800 °C in nitrogen increased the effective permittivity to 15.6−21.0 and decreased the rechargeable trap density. Praseodymium silicate films may be applied after annealing as dielectric layers in capacitive structures.

Introduction

Praseodymium oxide has been studied for different applications, such as components of varistor ceramic materials,[1,2] as photocatalytically active material,[3] as anode coatings for organic light-emitting diodes,[4] or as interface layers for improving Al/GaAs Schottky junction characteristics.[5] Praseodymium oxide has also been used to modify electronic and structural characteristics of mixed oxides such as HfO_2−$YO_{1.5}$−$PrO_{1.5}$,[6] ZrO_2−PrO_x mixtures,[7] or $PrTiO_x$.[3,8] In addition, praseodymium oxide is a high-permittivity (high *k*) dielectric oxide and is a promising alternative for SiO_2 in complementary metal-oxide-semiconductor (MOS) devices.[9]

It has been reported that stoichiometric Pr_2O_3[10,11] and PrO_2 films[12] can be grown epitaxially by molecular beam epitaxy (MBE) on single-crystal silicon, providing an electronically high-quality interface with low defect density and absence of interface reactions. Otherwise, praseodymium possesses a variable oxidation state with accompanying variable oxide stoichiometry, $PrO_{2-\delta}$.[13] Variations in the stoichiometry of PrO_x thin films, in particular the oxygen deficiency in relation to PrO_2, induce large variations in conductivity, allowing the recognition of space-charge limited and/or Schottky conduction mechanisms.[14−17] The energy gap of PrO_x films is lower (2−3.6 eV)[18,19] than that of another prospective high *k* oxide candidate, HfO_2 (5−6 eV), which usually would allow higher conductivity. Moreover, PrO_x films have a rather small conduction band offset (1 eV) that should serve as a charge barrier

* To whom correspondence should be addressed. Also at: University of Tartu, Institute of Experimental Physics and Technology, Tähe 4, EE−51010 Tartu, Estonia, E-mail: kaupo.kukli@ut.ee, kaupo.kukli@helsinki.fi.

† Department of Chemistry, University of Helsinki.

‡ Accelerator Laboratory, University of Helsinki.

§ University of Liverpool and Epichem Limited.

Freescale Semiconductor, Inc.

¶ Also at: Katholieke Universiteit Leuven, Instituut voor Kern- en Stralingsfysica, Celestijnenlaan 200D, B-3001 Leuven, Belgium.

(1) Horio, N.; Hiramatsu, M.; Nawata, M.; Imaeda, K.; Torii, T. *Vacuum* **1998**, *51*, 719.

(2) Nahm, C.-W. *J. Eur. Ceram. Soc*. **2003**, *23*, 1345.

(3) Hwang, D. W.; Lee, J. S.; Li, W.; Oh, S. H. *J. Phys. Chem. B* **2003**, *107*, 4963.

(4) Qiu, C.; Chen, H.; Xie, Z.; Wong, M.; Kwok, H. S. *Appl. Phys. Lett*. **2002**, *80*, 3485.

(5) Lin, J.; Hwu, M.-J.; Chang, L. B. *Jpn. J. Appl. Phys*. **1998**, *37*, L1437.

(6) Kalinina, M. V.; Tikhonov, P. A. *Technol. Phys. Lett*. **1997**, *23*, 257.

(7) Corradi, A. B.; Bondioli, F.; Ferrari, A. M. *Chem. Mater*. 4550, *13*, 4550.

(8) Jeon, S.; Hwang, H. *Appl. Phys. Lett*. **2002**, *81*, 4856.

(9) Osten, H. J.; Liu, J. P.; Gaworzewski, P.; Bugiel, E.; Zaumseil, P. *Technol. Dig. Int. Electron Dev. Meeting*; 2000; 653.

(10) Osten, H. J.; Liu, J. P.; Bugiel, E.; Müssig, H. J.; Zaumseil, P. *Mater. Sci. Eng. B* **2001**, *87*, 297; Osten, H. J.; Liu, J. P.; Bugiel, E.; Müssig, H. J.; Zaumseil, P. *J. Cryst. Growth* **2002**, *235*, 229; Osten, H. J.; Liu, J. P.; Müssig, H.-J.; Zaumseil, P. *Microelectron. Reliab*. **2001**, *41*, 991.

(11) Nigro, R. L.; Raineri, V.; Bongiorno, C.; Toro, R.; Malandriano, G.; Fragalà, I. L. *Appl. Phys. Lett*. **2003**, *83*, 129.

(12) Müssig, H.-J.; Dąbrovski, J.; Ignatovich, K.; Liu, J. P.; Zavodinsky, V.; Osten, H. J. *Surf. Sci*. **2002**, *504*, 159.

(13) Kimura, S.; Arai, F.; Ikezawa, M. *J. Electron Spectrosc. Relat. Phenom. 78*, 135.

(14) Goswami, A.; Goswami, A. P. *Thin Solid Films* **1974**, *20*, S3.

(15) Dutta, C. R.; Barua, K. *Thin Solid Films* **1983**, *103*, 295.; Dutta, C. R.; Barua, K. *J. Phys. D: Appl. Phys*. **1981**, *14*, L179.

(16) Arakawa, T.; Kabumoto, A.; Shiokawa, J. *J. Less-Common Met.* **1986**, *115*, 281; Arakawa, T.; Kabumoto, A.; Shiokawa, J. *Thin Solid Films* **1984**, *120*, L69.

(17) Thangadurai, V.; Huggins, R. A.; Weppner, W. *J. Solid-State Electrochem*. **2001**, *5*, 531.

(18) Goswami, A.; Goswami, A. P. *Thin Solid Films* **1975**, *27*, 123.

(19) Dąbrovski, J.; Zavodinsky, V.; Fleszar, A. *Microelectron. Reliab*. **2001**, *41*, 1093.

10.1021/cm0401793 CCC: $27.50 © 2004 American Chemical Society
Published on Web 10/23/2004

between Si and the oxide. Nevertheless, the electrons in the narrow *f*-type conduction band of PrO_2 have large effective masses and thus, in the case of appropriate stoichiometry, provide low leakage despite the small band offset.[19] Epitaxially grown Pr_2O_3 on silicon has provided ultralow leakage and good reliability of dielectric properties.[9] For this reason, the formation of PrO_x films, as well as their dielectric properties and interfaces with silicon, has recently been investigated in great detail.[11,20−22]

There are a number of different routes to praseodymium oxide layers. Since the early physical vacuum evaporation methods and oxidation of the Pr metal layer,[14,16,18] advanced methods for the fabrication of stoichiometric Pr_2O_3 films have been introduced, comprising pulsed laser deposition (PLD)[21,22] and MBE[10,24] techniques. Such methods provide high-purity films, especially at high substrate temperatures on the order of 800 °C.[10,24] Pr_2O_3 films have also been grown by metal−organic chemical vapor deposition (MOCVD).[11] The metal β-diketonate precursors used have been Pr(hfa)$_3$·diglyme (H-hfa = 1,1,1,5,5,5-hexafluoro-2,4-pentadione, diglyme = $CH_3O(CH_2CH_2O)_2CH_3$) and Pr(tmhd)$_3$ (H-tmhd = 2,2,6,6,-tetramethyl-3,5-heptandione), resulting, respectively, in the growth of strongly fluorinated oxide and the pure oxide. The phase of MOCVD PrO_x was found to be critically dependent on the partial pressure of oxygen, with the Pr_2O_3 phase being formed in the absence of oxygen ($P_{O_2} = 10^{-3}$ Torr) at a high substrate temperature of 750 °C.[25] The use of Pr(thmd)$_3$ led to amorphous films below 650 °C, while mixtures of crystallized Pr_6O_{11} and Pr_2O_3 were obtained at higher temperatures.[26]

Recently, praseodymium oxide has been deposited by liquid injection MOCVD at substrate temperatures between 400 and 600 °C.[27] In that study, a novel praseodymium complex, Pr(mmp)$_3$ (mmp = $OC(CH_3)_2$-$CH_2O(CH_3)$), was used with O_2 as the oxygen precursor. In this case, the films were polycrystalline over the complete range of deposition temperatures with the Pr_6O_{11} phase predomination.

Besides chemical vapor deposition, atomic layer deposition (ALD) of rare-earth metal oxides has also gained attention,[28] although little has been reported to date in the scientific literature. Lanthanide β-diketonates have been used for the ALD of rare-earth oxides, such as Sc_2O_3,[29,30] La_2O_3,[31] and CeO_2.[32] The β-diketonate precursors are generally not reactive with water, and, when using ozone as an ALD reactant,[30−32] no ALD growth window can be found. The organometallic precursor $(C_5H_5)_3Sc$ (cyclopentadienyl) has also been investigated when using water as the oxidant, and this led to the deposition of Sc_2O_3 films of acceptable quality and crystallinity.[30] Further, although alkylamides such as $Hf(NR_2)_4$ have been successfully used in ALD,[33] the simple lanthanide alylamides $Ln(NR_2)_3$ are unstable and not volatile. However, the monomeric lanthanide tris-silylamides $Ln[N(SiMe_3)_2]_3$ are volatile and relatively stable.[34] Although these precursors deposit Ln-silicates by MOCVD,[35] it was hoped that surface exchange reactions would predominate over thermal decomposition at the lower temperatures typically employed by ALD, so that the $[N(SiMe_3)_2]$ group would be cleanly eliminated as the stable $(Me_3Si)_2NH$ species via the reaction between $Ln[N(SiMe_3)_2]_3$ and [OH].

In the present study, the ALD of PrO_x based films has been studied using the precursors $Pr[N(SiMe_3)_2]_3$ and H_2O. Thin PrO_x based films were deposited in the temperature range of 200−400 °C to investigate the features of film growth, formation of crystalline structure, and some effects of annealing on dielectric behavior of the films.

Experimental Section

The film growth experiments were carried out in a flow-type hot-wall ALD reactor F120.[36] To examine the changes in film properties upon changes in substrate temperature, PrO_x based films were deposited at 200, 250, 300, 350, and 400 °C from $Pr[N(SiMe_3)_2]_3$ and H_2O on 5 × 5 cm^2 *n*-Si(100) and borosilicate substrates. The $Pr[N(SiMe_3)_2]_3$ was transferred into the reactor under an inert atmosphere from a glovebox by means of a special transfer device held under an argon atmosphere. Inside the ALD reactor, $Pr[N(SiMe_3)_2]_3$ was evaporated from an open boat at 140 °C. The duration of the $Pr[N(SiMe_3)_2]_3$ pulse was, for the sample series fabricated at different substrate temperatures, held constant at 0.4 s while the H_2O pulse and purge times were all 0.5 s. To examine the ability of the $Pr[N(SiMe_3)_2]_3$ adsorption process to self-saturate, the $Pr[N(SiMe_3)_2]_3$ pulse length was varied between 0.2 and 0.8 s at 300 °C. Further, a series of films with variable thickness was deposited at 300 °C, using 150, 250, and 750 ALD cycles. Part of the films was grown on silicon substrates etched prior to deposition in 1% HF aqueous solution for ca. 30 s, without further rinsing in deionized water. Reference films were grown on silicon substrates that were RCA cleaned, being thus covered with a chemically grown 0.9−1.8 nm thick SiO_2 layer.

The refractive indexes and thicknesses of the films in the thickness range of 50−470 nm were evaluated from the transmission spectra measured by a Hitachi U2000 spectrophotometer.[37] The thicknesses of the films in the range of 9−50 nm were evaluated from X-ray reflection patterns measured with a Bruker D8 Advance X-ray diffractometer. The film structure was studied by means of a Philips MPD 1880 powder X-ray diffractometer using Cu Kα radiation and Bragg−

(20) Jeon, S.; Hwang, H. *J. Appl. Phys*. **2003**, *93*, 6393.
(21) Kanashima, T.; Sohgawa, M.; Kanda, H.; Ikeda, K.; Okuyama, M. *J. Korean Phys. Soc*. **2003**, *42*, S1357.
(22) Osten, H. J.; Bugiel, E.; Fissel, A. *Solid-State Electron.* **2003**, *47*, 2161.
(23) Wolfframm, D.; Ratzke, M.; Kouteva-Arguirova, S.; Reif, J. *Mater. Sci. Semicond. Process.* **2003**, *5*, 429.
(24) Fissel, A.; Olsten, H. J.; Bugiel, E. *J. Vac. Sci. Technol., B* **2003**, *21*, 1765.
(25) Nigro, R. L.; Toro, R.; Malandrino, G.; Raineri, V.; Fragalà, I. L. *Electrochem. Soc. Proc*. **2003**, *2003−08*, 915.
(26) Nigro, R. L.; Toro, R. G.; Malandrino, G.; Raineri, V.; Fragalà, I. L. *Adv. Mater*. **2003**, *15*, 1071.
(27) Aspinall, H. C.; Gaskell, J.; Williams, P. A.; Jones, A. C.; Chalker, P. R.; Marshall, P. A.; Bickley, J. F.; Smith, L. M.; Gritchlow, G. W.; *Chem. Vap. Deposition* **2003**, *9*, 235.
(28) Leskelä, M.; Ritala, M. *J. Solid-State Chem*. **2003**, *17*, 170.
(29) Meszaros-Szecsenyi, K.; Päiväsaari, J.; Putkonen, M.; Niinistö, L.; Pokol, G. *J. Therm. Anal.* **2002**, *69*, 65.
(30) Putkonen, M.; Nieminen, M.; Niinistö, J.; Niinistö, L.; Sajavaara, T. *Chem. Mater*. **2001**, *13*, 4701.
(31) Nieminen, M.; Putkonen, M.; Niinistö, L. *Appl. Surf. Sci*. **2001**, *174*, 155.
(32) Päiväsaari, J.; Putkonen, M.; Niinistö, L. *J. Mater. Chem*. **2002**, *12*, 1828.
(33) Kukli, K.; Ritala, M.; Sajavaara, T.; Keinonen, J.; Leskelä, M. *Chem. Vap. Deposition* **2002**, *8*, 199.
(34) Bradley, D. C.; Ghotra, J. S.; Hart, F. A. *J. Chem. Soc., Dalton Trans*. **1973**, 1021.
(35) Aspinall, H. C.; Gaskell, J.; Williams, P. A.; Jones, A. C.; Chalker, P. R.; Marshall, P. A.; Smith, L. M.; Critchlow, G. W. *Chem. Vap. Deposition* **2004**, *10*, 83.
(36) Suntola, T. *Thin Solid Films* **1992**, *216*, 84.
(37) Ylilammi, M.; Ranta-aho, T. *Thin Solid Films* **1993**, *232*, 56.

Brentano geometry. Transmission electron microscopy (TEM) was applied for imaging the cross-section of selected samples. Film composition was determined by time-of-flight elastic recoil detection analysis (TOF-ERDA),[38] using a 48 MeV $^{79}Br^{9+}$ projectile ion beam. In addition, secondary ion mass spectrometry (SIMS) was applied for selected samples to determine the uniformity of elemental composition.

Dielectric properties were measured after e-beam evaporation of aluminum shadow masked electrodes with the effective electrode area of 0.204 mm^2. After film deposition, the backsides of the silicon substrates were etched in hydrofluoric acid and metallized by evaporating a 100−150 nm thick Al layer. Thus, the electrical measurements were carried out on Al/HfO_2/*n*-Si(100)/Al or Al/HfO_2/SiO_2/*n*-Si(100)/Al capacitor structures. Capacitance−voltage curves were recorded using a HP 4284A precision LCR meter in a two-element series circuit mode. The stair sweep voltage step was 0.05 V. The period between voltage steps was 0.5 s. The AC voltage applied to the capacitor was 0.05 V, while the frequency of the ac signal was held at 500 kHz. The current−voltage curves were measured with a Keithley 2400 Source Meter in the stair sweep voltage mode while the voltage step used was 0.02−0.05 V. All measurements were carried out at room temperature.

Results and Discussion

Film Growth and Structure. The adsorption of Pr[$N(SiMe_3)_2]_3$ was not entirely self-limiting. At 300 °C, the growth rate was increasing along with the increase in the Pr[$N(SiMe_3)_2]_3$ pulse length. In the case of a Pr[$N(SiMe_3)_2]_3$ pulse length of 0.2, 0.4, and 0.8 s, the average film growth rate was 0.015, 0.026, and 0.034 nm/cycle. At 200 °C, the film growth rate was as high as 0.26 ± 0.02, 0.29 ± 0.10, and 0.30 ± 0.12 nm/cycle, when the Pr[$N(SiMe_3)_2]_3$ pulse length was 0.4, 0.8, and 1.2 s. Thus, some decomposition takes place, but the process is still rather slow even at 300 °C. A higher growth temperature, 350 °C, caused considerably stronger decomposition and strongly affected the film thickness profile. At 400 °C, virtually no film could be deposited; all the precursor was decomposed in the source tube before reaching the substrate.

In a series of the samples grown at variable substrate temperatures with 0.4 s Pr precursor pulse length, 466, 99, and 78 nm thick films were obtained at 200, 250, and 300 °C, using 4070, 3000, and 3000 growth cycles and thus growing with the rates of 0.11, 0.033, and 0.026 nm/cycle, respectively. At 250−300 °C, the film thickness varied not more than 1−2.5% along the gas flow direction, measured at 1.5−3.5 cm distances from the leading edge of the substrate. The refractive indexes of the films grown at 200, 250, and 300 °C were 1.85 ± 0.03, 1.85 ± 0.03, and 1.78 ± 0.02, respectively, being comparable with the values characterizing thermally evaporated films.[18]

All the films were amorphous in the as-deposited state. Annealing at 800 °C did not suffice for crystallization. The peaks at 25.37, 27.60, and 31.44° in the XRD pattern (Figure 1) of the film grown at 350 °C and annealed at 1000 °C in N_2 for 1 min could be assigned as 400, −210, and 012 reflections of monoclinic Pr_2O_3.[39] However, impurities and other phases complicate the phase assignments. The peak visible at 42.9° does not match with the Pr_2O_3 phase, although the next, the smallest, peak at 48.47° corresponds to the interplanar distance 1.88 Å and can thus be assigned as the 31-4 or 413 reflection of monoclinic Pr_2O_3 with a slight shift possibly caused by impurity-induced strains. PrO_2 and Pr_6O_{11} can be excluded on the basis of XRD results of the annealed films. The peaks at 42.9° (d = 2.11 Å), 25.37° (d = 3.51 Å), 27.7° (d = 3.23 Å), 31.44° (d = 2.84 Å), and 48.47° belong, instead of Pr_2O_3, to 113, 002, 102, 112, and 213 reflections of $Pr_{9.33}(SiO_4)_6O_2$,[40,41] respectively. In the highly impure films grown at 200 °C and annealed at 1000 °C (Figure 1), phase determination was not possible. Possibly, these films could contain also some amounts of carbonates.

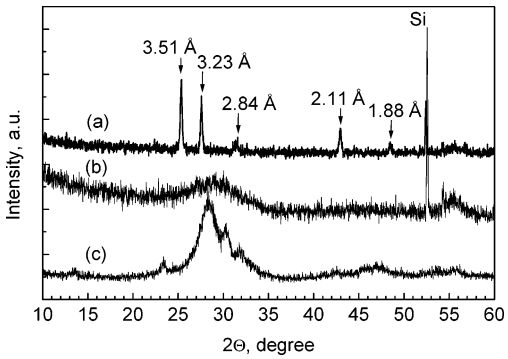

Figure 1. X-ray diffraction patterns of PrO_x films deposited at 350 °C and annealed at 1000 °C in N_2 for 1 min (a), as deposited at 350 °C (b), deposited at 200 °C, and annealed at 1000 °C in N_2 for 5 min (c). Labels denote interplanar distances corresponding to the apparent diffraction peaks. For the phase description, see text.

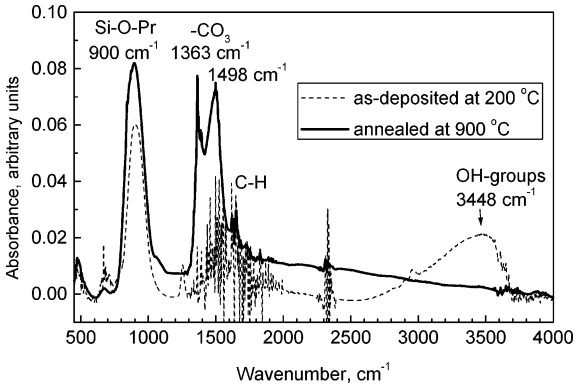

Figure 2. FTIR spectra of 360−370 nm thick PrO_x film grown at 200 °C with Pr precursor pulse length of 0.4 s using 1400 growth cycles. Annealing was carried out at 900 °C in a vacuum under nitrogen flow during 5 min.

FTIR analysis carried out on the films grown at the lowest temperature examined, 200 °C, (Figure 2) confirmed the existence of carbon contributing to the elemental composition of low-temperature films. Carbonate formation in such a kind of high-permittivity rare-earth oxides has earlier been reported by Gougousi et al.,[42] Kosola et al.,[43] and Nieminen et al.[31] In the

(38) Jokinen, J.; Haussalo, P.; Keinonen, J.; Ritala, M.; Riihelä, D.; Leskelä, M. *Thin Solid Films* **1996**, *289*, 159.

(39) Joint Committee of Powder Diffraction Data, PDF Card 22−880.

(40) Kolitsch, U.; Seifert, H. J.; Aldinger, F. *J. Solid State Chem.* **1995**, *120*, 38.

(41) Joint Committee of Powder Diffraction Data, PDF Card 23−1389.

(42) Gougousi, T.; Niu, D.; Ashcraft, R. W.; Parsons, G. N. *Appl. Phys. Lett.* **2003**, *83*, 3543.

(43) Kosola, A.; Putkonen, M.; Johansson, L.-S.; Niinistö, L. *Appl. Surf. Sci.* **2003**, *211*, 102.

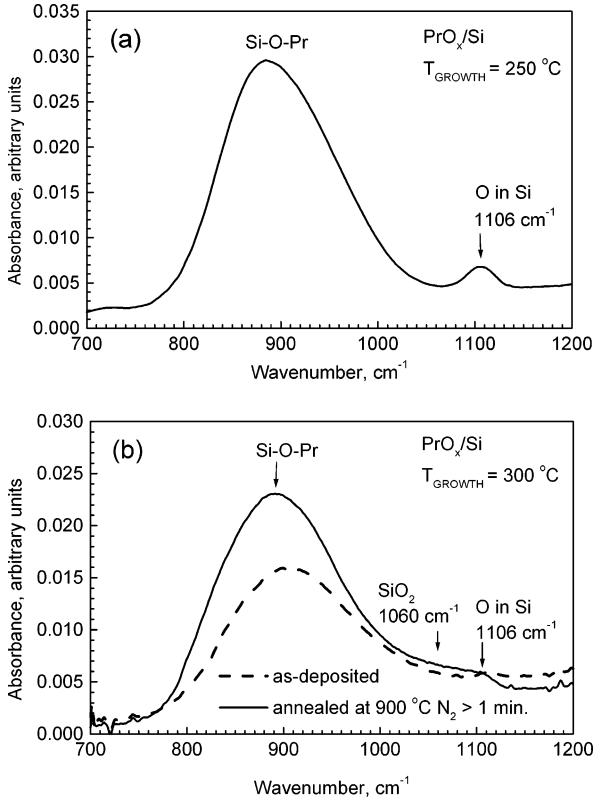

Figure 3. FTIR spectra of 100−150 nm thick PrO_x film grown at 250 (a) and 300 °C (b) with Pr precursor pulse length of 0.4 s. Annealing was carried out at 900 °C in a vacuum under nitrogen flow during 5 min.

present study, the C−H vibration bands apparent in the wavenumber range 1400−2000 cm^{-1} (Figure 2) disappeared upon annealing, along with the appearance of carbonate bands centered at 1363 and 1498 cm^{-1}. Hydrogen was annealed out, since, besides C−H, the OH band ranging between 3300 and 3600 cm^{-1} also obviously vanished due to the annealing procedure. In addition, the FTIR peak at 900 cm^{-1}, attributable to Si-O−Pr bonds,[44] increased upon annealing. The peak at 1270 cm^{-1} (Figure 2) might refer to the Si−C bonds,[45] but other peaks characteristic of Si−C oscillations,[45,46] such as 781 or 825−898 cm^{-1}, either did not appear or overlapped with compositionally more feasible Si−O−Pr peaks. Thus, the crystal structure is rather a mixture of silicates and carbonates. In the films grown at higher temperatures, 250 and 300 °C, the carbonate peak did not appear as prominently as in the films grown at 200 °C. This might refer to the somewhat higher purity, but also to the possibility that these films may not contain that much excess oxygen (as OH groups or in water) to form carbonates. In some of the films, the growth of interfacial SiO_2 upon annealing was detected as the formation and increase of the FTIR signal between 1000 and 1100 cm^{-1} (Figure 3). The growth of interfacial oxide was still of minor importance according to FTIR.

Figure 4 demonstrates the TEM images of a PrO_x film grown at 300 °C on HF-etched silicon. The TEM studies revealed the growth of a uniform, amorphous film. No

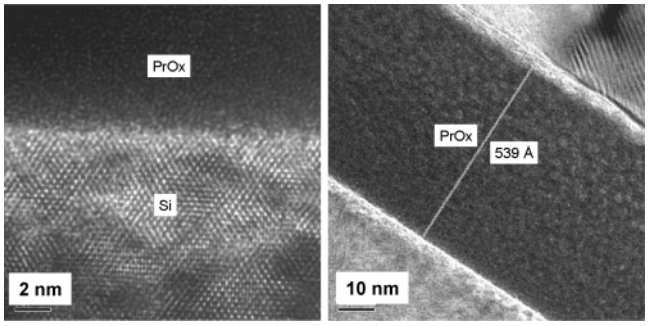

Figure 4. Transmission electron microscope images of a PrO_x film grown at 300 °C on HF-etched Si(100).

pronounced formation of interfacial SiO_2 or a Si-rich PrO_x layer was detected by TEM. This can also mean that silicon is quite evenly distributed throughout the film thickness and visual distinction of the interfacial layer becomes complicated. However, the TEM supports the FTIR results, according to which the interfacial layer silicon oxide growth is not as pronounced nor of considerable thickness in as-deposited films.

Film Composition. The elemental composition of the PrO_x based films grown at 200, 250, and 300 °C was determined by TOF-ERDA (Table 1). In these films, the analysis revealed O/Pr ratios of 2.6:1, 2.3:1, and 2.5:1, respectively, in the as-deposited state. Thus, the films contained considerable amounts of excess oxygen. In addition, the films contained 36, 21, and 12 at. % hydrogen and 4, 6, and 10 at. % silicon, respectively, averaged throughout the film thickness. Nitrogen content was below any detection limit of TOF-ERDA and could not be observed, in practice. Both silicon and hydrogen are constituents of the precursors, and their residual content can thus vary with the deposition temperature. It is interesting to note that the amount of hydrogen in the films decreased with increasing deposition temperature, whereas the amount of silicon increased. This suggests that some thermal decomposition of $[-N(SiMe_3)_2]$ is occurring. There is also a possibility that $[-N(SiMe_3)_2]$ may hydrolyze to form silanol species such as Me_3SiOH, and silanols have been shown to be effective precursors to metal silicates in both MOCVD[47] and ALD.[48] Furthermore, silicon can diffuse out of the substrate into the metal oxide film, especially after the annealing procedure, and significantly increase the amount of silicon concentration in the film bulk. The increased hydrogen contents at lowered substrate temperatures are characteristics of other metal oxides also grown by atomic layer deposition, being observed in the case of HfO_2[49] and ZrO_2[50] grown from alkoxide or halide precursors. Thus, since high hydrogen contents have been observed in the case of hydrogen-free metal precursors with H_2O reactants, it appears quite reasonable to connect hydrogen to hydroxyl residues. The carbon content detected was

(44) Ono, H.; Katsumata, T. *Appl. Phys. Lett*. **2001**, *78*, 1832.
(45) Hu, J. C.; Wu, C. W.; Gau, W. C.; Chen, C. P.; Chen, L. J.; Li, C. H.; Chang, T. C.; Chu, C. J. *J. Electrochem. Soc*. **2003**, *150*, F61.
(46) Quian, J.-M.; Wang, J.-P.; Qiao, G.-J.; Jin, Z.-H. *J. Eur. Ceram. Soc*. **2004**, *24*, 3251.
(47) Roberts, J. L.; Marshall, P. A.; Jones, A. C.; Chalker, P. R.; Bickley, J. F.; Williams, P. A.; Taylor, S.; Smith, L. M.; Critchlow, G. W.; Schumacher, M.; Lindner, J. *J. Mater. Chem*. **2004**, *14*, 391.
(48) Gordon, R. G.; Becker, J.; Hausmann, D.; Suh, S. *Chem. Mater*. **2001**, *13*, 2463.
(49) Kukli, K.; Ritala, M.; Leskelä, M.; Sajavaara, T.; Keinonen, J.; Jones, A. C.; Roberts, J. L. *Chem. Mater*. **2003**, *15*, 1722.
(50) Kukli, K.; Ritala, M.; Aarik, J.; Uustare, T.; Leskelä, M. J. *Appl. Phys.* **2002**, *92*, 1833.

Table 1. TOF-ERDA Results (elemental composition) of Selected PrO_x Films Grown by ALD

growth temp (°C)	status	O, at. %	Pr, at. %	H, at. %	Si, at. %	C, at. %	Pr/Si/O
200	as deposited	41 ± 2	16 ± 2	36 ± 4	4 ± 1	2.8 ± 0.3	1:0.3:2.6
250	as deposited	49 ± 4	21 ± 3	21 ± 5	6 ± 2	2.6 ± 0.5	1:0.3:2.3
250	annealed in N_2 at 800 °C for 3-4 min	63 ± 4	26 ± 3	<0.5	7 ± 2	2.5 ± 0.5	1:0.3:2.4
300	as deposited	54 ± 5	22 ± 3	12 ± 3	10 ± 4	2.8 ± 1.0	1:0.5:2.5
300	annealed in air at 800 °C for 3-4 min	62 ± 4	22 ± 3	2 ± 1	12 ± 4	2.5 ± 0.5	1:0.5:2.8

relatively low (2.5−2.8 at. %) and did not change after annealing.

The SIMS analysis revealed quite uniform oxygen and praseodymium concentration in 50 and 80 nm thick samples grown at 250 and 300 °C (Figure 5). The distribution of carbon was less uniform and generally decreased toward the film surface at both growth temperatures. However, the carbon content increased at the film/substrate interface, leading to a peak in the SIMS profile. Although SIMS peaks at interfaces can also be due to matrix effects when sputtering across different materials, comparing the 250 and 300 °C SIMS carbon profiles indicates that the 300 °C deposition temperature leads to greater amounts of carbon near the Si substrate interface. It is worth noting that the residual concentration peaks observed at the film/substrate interface as well as at the film surface are a rather general problem and have been observed in ALD-grown[51] and MOCVD oxide films.[52] At solid−solid interfaces, this could be connected to the larger structural disorder naturally present at the incommensurate (nonepitaxial) junctions. Larger structural disorder could possibly accommodate larger amounts of substitutional and interstitial impurities. The impurity content further diminishes upon the growth in the oxide layer thickness and densification of the material. The surface carbon can arise from species adsorbing during storage in the ambient air. Also, there were nonuniformities in the silicon concentration profile. In a manner similar to the carbon level, the amount of Si decreased toward the film surface but gave a concentration peak at the film surface. This peak might be caused by the incomplete surface reactions and unreacted precursor ligands, in addition to the diffusion and collection of silicon at the interface or surfaces as defective boundaries.

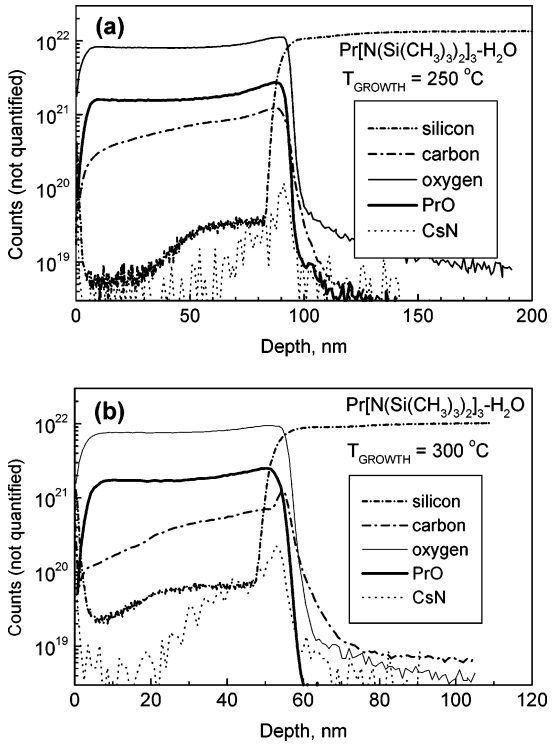

Figure 5. Secondary ion mass spectrometry composition profiles of PrO_x films as deposited at 250 (a) and 300 °C (b) on Si(100) substrates.

The heat treatment changed the film composition to a certain extent. Annealing at 800 °C in ambient nitrogen and ambient air for 3−4 min reduced the amount of residual hydrogen (Table 1). The O/Pr atomic ratios after annealing were 2.4:1 and 2.8:1, remaining rather far from the PrO_2 or Pr_2O_3 stoichiometry. This allows the conclusion that the excess oxygen is bound to silicon, and the relative content of silicon was not reduced, but actually increased upon annealing. The films are thus praseodymium-rich mixtures of PrO_x and SiO_x. It is worth noting that according to literature the Pr_2O_3/Si interface is very reactive and Si−O−Pr bonds easily form and/or the SiO_2 layer grows.[12,53] Moreover, substrate silicon diffuses eagerly into Pr_2O_3, especially upon heat treatments.[54,55] Pr^{3+} is characterized by a large ionic radius, causing a less dense Pr_2O_3 lattice favoring the (silicon) diffusion and more pronounced Si−O−Pr or Si−O−Si bond formation when compared to Ta_2O_5 and ZrO_2.[44] Furthermore, the structures of monoclinic Pr_2O_3 and $Pr_{9.33}(SiO_4)_6O_2$ are identical,[40] which relates to the ability or probability of forming solid solutions, or mixtures, as described above (Figure 1). It has actually been suggested that there hardly exists any monoclinic praseodymium oxide polymorph and that praseodymium silicate is formed during the synthesis in the quartz-walled reaction zones and susceptors, instead.[40]

One can estimate the phase composition on the basis of elemental concentration data represented by Table 1, complemented by XRD and FTIR results indicating the presence (formation) of silicate and carbonates. One can assume here that the film essentially consists of a mixture of of $Pr_{9.33}(SiO_4)_6O_2$ and the carbonate compound $Pr_2O_2CO_3$. If the amount (12%) of silicon measured in annealed film grown at 300 °C is taken as the reference value, then the relative elemental composition of $Pr_{9.33}(SiO_4)_6O_2$ comprises 12% Si, 18.66% Pr, and 52%

(51) Scarel, G.; Ferrari, S.; Spiga, S.; Wiemer, C.; Tallarida, G.; Fanciulli, M. *J. Vac. Sci. Technol., A* **2003**, *21*, 1.
(52) Schaeffer, J.; Edwards, N. V.; Liu, R.; Roan, D.; Hradsky, B.; Gregory, R.; Kulik, J.; Duda, E.; Contreras, L.; Christiansen, J.; Zollner, S.; Tobin, P.; Nguyen, B.-Y.; Nieh, R.; Ramon, M.; Rao, R.; Hegde, R.; Rai, R.; Baker, J.; Voigt, S. *J. Electrochem. Soc.* **2003**, *150*, F67.
(53) Schmeisser, D.; Müssig, H.-J. *Solid-State Electron.* **2003**, *47*, 1607.; Schmeisser, D. *Mater. Sci. Semicond. Process.* **2003**, *6*, 59.
(54) Goryachko, A.; Liu, J. P.; Krüger, D.; Osten, H. J.; Bugiel, E.; Kurps, R.; Melnik, V. *J. Vac. Sci. Technol., A* **2002**, *20*, 1860.
(55) Wang, Z. M.; Wu, J. X.; Ma, M. S.; Chen, W.; Fang, Q.; Zhang, J.-Y. *Microelectron. Eng.* **2003**, *66*, 608.

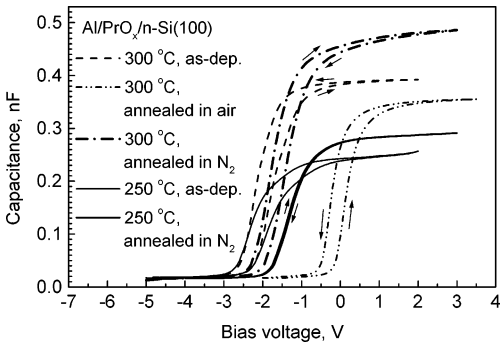

Figure 6. Capacitance−voltage curves of Al/PrO_x/Si capacitors based on 100 and 78 nm thick PrO_x films grown on HF-etched Si(100) at 250 and 300 °C, respectively, in as-deposited and annealing states. Labels denote the growth temperature and annealing ambient. Annealing was carried out at 800 °C for 1 min in N_2 and 3−4 min in air.

O, while the corresponding composition of $Pr_2O_2CO_3$ is 2.5% C (measured), 5% Pr, and 12.5% O. When summarized, the total relative composition of the mixture is then 23.6% Pr, 12% Si, 2.5% C, and 64.5% O; these values indeed overlap with the elemental composition of the films grown at 300 °C and annealed at 800 °C (Table 1). The $Pr_2O_2CO_3$ could, in principle, be an intermediate formed after temperature-enhanced release of CO_2 from the initially formed $Pr_2(CO_3)_2$. The $Pr_2O_2CO_3$ might further release CO_2 and thus be a precursor for Pr_2O_3. However, the carbon can obviously not be completely annealed out at 800 °C, and the carbonate contribution is retained. Nevertheless, some PrO_2 might be expected in the annealed films initially grown at 250 °C. In these films, namely, the measured silicon and carbon contents allow 7% Si, 10.89% Pr, and 30.39% O for $Pr_{9.33}(SiO_4)_6O_2$ and 2.5% C, 5% Pr, and 12. 5% O for additive $Pr_2O_2CO_3$. Together, it makes 15.89% Pr and 42.8% O in the mixture of silicate and carbonate, leaving 10.1% Pr and 20.2% O; these two values match well with PrO_2 stoichiometry. It is to be noted that this is valid for the annealed films, and analogous calculations for as-deposited films do not result in the stoichiometry of defined compounds.

Dielectric Properties. The dielectric behavior was first evaluated for the relatively thick (99 and 78 nm) films grown at 250 and 300 °C. Figure 6 demonstrates the Capacitance−voltage (C−V) curves of these films. The effective permittivity calculated from accumulation capacitance, using a simple parallel-plate capacitor model, was 13.7 and 15.9, respectively. Multiple back-and-forth bias voltage sweeps caused some shifts in flat-band voltage, referring to some development of rechargeable and/or oxide trap density; in particular, this referred to an increase in the density of negative charge in the films. Electron trapping upon multiple voltage sweeps is thus very likely. The hysteresis direction was counterclockwise, also referring to the dominance of electron trapping instead of mobile ion conduction.[56−58]

Annealing at 800 °C in nitrogen did not lead to the crystallization of the films but, at the same time, clearly increased the capacitance. The effective permittivity of the films grown at 250 and 300 °C was increased up to 15.6 and 21.0, respectively. Essential effects of nitrogen annealing also were the narrowing of the hysteresis in C−V curve of the film grown at 250 °C and a change in the hysteresis direction from counterclockwise to clockwise in both films. A change in hysteresis direction refers to a change in dominant conduction mechanism, for example, from electron injection/conduction and trapping to mobile ion conduction.[56] It is quite interesting that annealing in air did not change the hysteresis direction. Annealing in an air atmosphere shifted the flat-band voltage strongly (by 2−3 V) toward positive bias voltage and more close to the predicted flat-band voltage value (−0.3−0.4 V),[57] but decreased the capacitance. Capacitance could decrease for two reasons: growth of an interfacial SiO_2 layer and diffusion of Si into the metal oxide followed by the oxidation of the diffused Si. The differences observed electrically after nitrogen and air (oxygen-assisted) annealings could be connected to the differences in the microstructures formed. For instance, for slightly oxygen-deficient praseodymium oxide, the influence of the annealing atmosphere on phase transitions has been studied, and the restructuring of PrO_2 proceeds differently.[59] In the case of composite and/or $Pr_{9.33}(SiO_4)_6O_2$ films such as those obtained in the present study, interdependence between structure, annealing effect, and conduction mechanisms should be characterized in more detail, but this remains beyond the scope of this work.

It is to be noted that the dielectric permittivity values achieved in the present study remained lower compared to the characteristic values of Pr_2O_3 grown by MBE in the temperature range 800−1000 °C.[24] For the latter films, effective dielectric permittivities as high as 30 were measured. Also, the permittivity of MOCVD Pr_2O_3 films grown at temperatures exceeding 650 °C[11,26] has been higher (25) than that obtained in the present study. On the other hand, the permittivity of the films in this study exceeds that obtained by physical vapor deposition.[14] As noted above, the lower permittivity may also be due to the increased silicon content or even the formation of films with structure and composition corresponding to $Pr_{9.33}(SiO_4)_6O_2$.

Some thinner PrO_x based films were also prepared for the dielectric measurements at 300 °C, using 750, 250, and 150 growth cycles. The thicknesses of the films were 53, 18, and 9 nm, respectively. This temperature was chosen due to its consistency with the most commonly used ALD regimes,[60−62] keeping in mind further possibilities to create multilayered structures with other materials such as HfO_2. Figure 7 depicts some selected C−V curves of Al/PrO_x/Si and Al/PrO_x/SiO_2/Si capacitor structures with PrO_x layers of variable thickness. The accumulation capacitance was naturally correlated to the film thickness. It can be seen that the C−V curves demonstrated rather considerable hysteresis in the case

(56) Schröder, D. K. *Semiconductor Material and Device Characterization*, 2nd ed.; J. Wiley and Sons, Inc.: New York, 1998; p 350.
(57) Sze, S. M. *Physics of Semiconductor Devices*, 2nd ed.; Wiley: New York, 1981; p 397.
(58) Hori, T. *Gate Dielectrics and MOS ULSIs, Principles, Technologies and Applications*; Springer-Verlag: Berlin, 1997; p 40.
(59) Wakiya, N.; Chun, S.-Y.; Saiki, A.; Sakurai, O.; Shinosaki, K.; Mizutani, N. *Thermochim. Acta* **1998**, *313*, 55 1998.
(60) Baldovino, S.; Nokhrin, S.; Scarel, G.; Fanciulli, M.; Graf, T.; Brandt, M. S. *J. Non-Cryst. Solids* **2003**, *322*, 168.
(61) Kim, H.; McIntyre, P. C.; Saraswat, K. C. *J. Mater. Res.* **2004**, *19*, 643.
(62) Jeon, S.; Yang, H.; Park, D.-G.; Hwang, H. *Jpn. J. Appl. Phys.* **2002**, *41*, 2390.

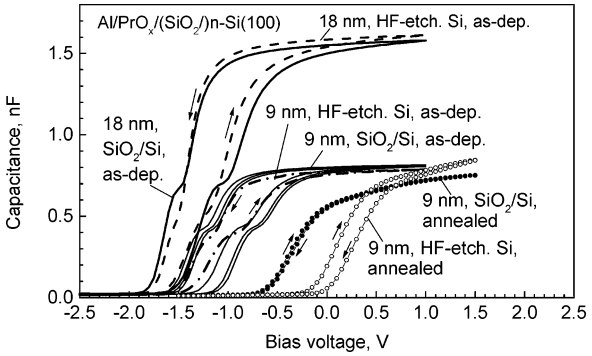

Figure 7. Capacitance−voltage curves of Al/PrO_x/Si capacitors based on 18 and 9 nm thick PrO_x films grown on etched or RCA-cleaned Si(100) at 300 °C in as-deposited and annealing states. Annealing was carried out at 900 °C for 1 min in N_2.

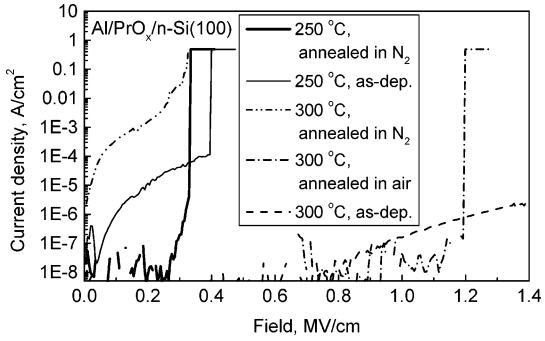

Figure 8. Leakage current density vs electric field curves of Al/PrO_x/Si capacitors based on 100 and 78 nm thick PrO_x films grown on HF-etched Si(100) at 250 and 300 °C, respectively, in as-deposited and annealing states. Labels denote the growth temperature and annealing ambient. Annealing was carried out at 800 °C for 1 min in N_2 and 3−4 min in air. Electrons were injected from substrate.

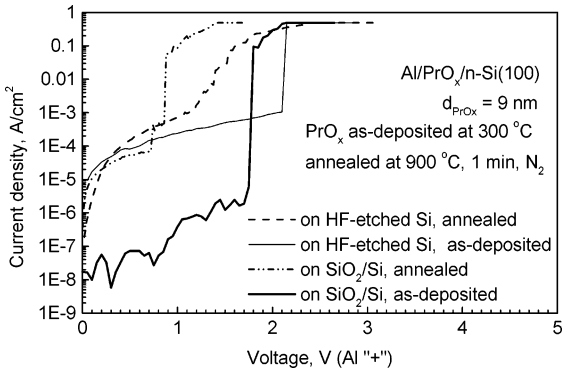

Figure 9. Leakage current density vs electric field curves of Al/PrO_x/Si capacitors based on 9 nm thick PrO_x films grown on HF-etched and RCA-cleaned Si(100) at 300 °C. Labels denote the growth temperature and annealing ambient. Annealing was carried out at 900 °C for 1 min in N_2. Electrons were injected from substrate.

of both HF-etched Si substrate and Si substrate covered with SiO_2. The hysteresis width can be regarded as a measure of the electron and hole trapping in the oxide due to high defect density.[63] In addition, rather pronounced kinks, or "shoulders", became observable in the depletion regions of the C−V curves, that is, during the transition of voltage sweeps from the minimum capacitance values to the plateau of maximum (accumulation) capacitances. This kink can be regarded as a sign of increased density of interface traps.[64] The 9 nm thick film possessed the capacitance equivalent oxide thickness value of 4.4−4.5 nm, which is quite close to the value obtained in the films grown by PLD[21] at rather low substrate temperatures compared to those used for MBE. Similarly to the 78−100 nm thick films, the 9−53 nm thick films also demonstrated changes in the C−V hysteresis direction upon nitrogen annealing, this time at 900 °C, indicating that the structural modifications and dielectric performance observed in thick films are relevant in the thin films, too. At the same time, "shoulder"-like features disappeared. Essential differences were not observed between the films as deposited on HF-etched and RCA-cleaned silicon (SiO_2/Si)). In the case of annealed films, hysteresis vanished more easily in the films grown on HF-etched silicon. On the other hand, this effect may also be related to the faster detrapping of charge carriers from the disorder-induced interface and fixed charge traps, responsible for the hysteresis phenomenon, which are of much higher density compared to the films grown on SiO_2/Si. In this case, the hysteresis reduction can be accompanied by a decrease in the film resistivity.

Figures 8 and 9 describe the leakage properties of selected relatively thick and thin films, respectively. In the film grown at 250 °C, the leakage currents generally decreased after annealing (Figure 8), while in the film grown at 300 °C the leakage current was increased or the breakdown resistance decreased (Figures 8 and 9). This is valid for both kinds of substrates, HF-etched Si and SiO_2/Si. Typical breakdown fields varied between 0.6 and 1.2 MV/cm. It is possible that annealing mainly reduces the relatively high hydrogen concentration in the films grown at 250 °C (Table 1), densifies the films not affecting the compositional homogeneity, and decreases the leakage current density. At the same time, in the films grown at 300 °C the hydrogen content is lower and the silicon content is higher than in the films grown at 250 °C (Table 1, Figure 5), possibly enabling phase separation upon annealing, accompanied by higher defect density and higher leakage. The leakage behavior for 300 °C films is similar regardless of the film thickness, since a similar increase of the leakage current upon anneal was also observed in the 9−18 nm thick films (Figure 9) and 52 nm thick films (not shown).

In conclusion, PrO_x based films, grown by ALD from $Pr[N(SiMe_3)_2]_3$ and H_2O, contained considerable amounts of both residual hydrogen and residual or diffused silicon. Crystallization of these films took place after annealing at 900−1000 °C, and X-ray diffraction data indicated that the films were $Pr_{9.33}(SiO_4)_6O_2$. The effective permittivity of as-deposited films was in the range of 14−16.0. Annealing the films at 800 °C in nitrogen increased the effective permittivity to 15.6−21.0 and decreased the rechargeable trap density. The praseodymium silicate films deposited from $Pr[N(SiMe_3)_2]_3$ may be applied after annealing as dielectric layers in capacitive structures due to their relatively high permittivity, low leakage, and high crystallization temperature.

(63) Wang, J. C.; Shie, D. C.; Lei, T. F.; Lee, C. L. *Appl. Phys. Lett.* **2004**, *84*, 1531.
(64) Kim, H.; McIntyre, P. C.; Saraswat, K. C. *Appl. Phys. Lett.* **2003**, *82*, 106.

CM0401793